Applied Physics B (2023) 129:46
https://doi.org/10.1007/s00340-023-07979-z

Applied Physics B
Lasers and Optics

RESEARCH

Analogy of harmonic modelocked pulses to trapped Brownian particles improves laser performance

Mesut Laçin[1] · Paul Repgen[1] · Aladin Şura[2] · Çağrı Şenel[3] · Fatih Ömer Ilday[1,2,4]

Received: 6 January 2023 / Accepted: 18 January 2023 / Published online: 28 February 2023

Abstract
High-repetition-rate ultrafast lasers are needed for diverse applications. Harmonic modelocking, where multiple identical, equidistant pulses circulate in the cavity, reaches beyond the practical limitations of reducing the cavity length. However, it suffers from stochastic deviations that manifest as supermodes in the radio-frequency spectrum and difficulties in maintaining the same harmonic state, often coupled with trade-offs in pulse energy, duration, or noise performance. Here, we first show that deviations in the temporal positions of the pulses contribute disproportionately more to the supermodes than deviations in their amplitudes. Then, we argue that these fluctuations are analogous to those of trapped Brownian particles. This analogy reveals that supermodes are suppressed by stronger spectral filtering, which corresponds to fluid viscosity, and higher pulse energy reduces the noise, akin to lower temperature. Guided by this intuitive picture, we construct a Yb-fibre laser incorporating strong filtering and high intracavity energies by limiting nonlinear polarisation evolution to a short section of ordinary fibre. The rest of the all-fibre cavity comprises polarisation-maintaining fibre, which additionally improves environmental robustness. We report record-high supermode suppression ratios, reaching 80 dB, excellent long-term and environmental stability, and pulse energy, duration, and noise characteristics that are similar to fundamentally modelocked lasers.

1 Introduction

The first time a laser was modelocked in 1964, it had a repetition rate of 56 MHz [1]. Over the six decades that followed, every parameter of a *typical* modelocked laser except the repetition rate has improved by orders of magnitude. Today, the vast majority of modelocked lasers continue to operate with repetition rates within a factor of two or three of the historical value of 56 MHz. Yet, applications like ablation-cooled material processing [2] or nonlinear bioimaging [3] require much higher repetition rates.

In conventional or fundamental modelocking, there is a single pulse in the cavity; the repetition rate is given by the speed of light divided by the cavity length. Therein lies the limitation: The cavity cannot be shrunk easily due to practical considerations. Many applications demand nanojoule-level pulse energies, and the average power is the product of the pulse energy and the repetition rate. This makes scaling without sacrificing the pulse energy even more difficult because high-power cavities cannot be very short. The commendable progress in bulk solid state and semiconductor lasers [4] notwithstanding, the prospects of high-power, high-repetition-rate fundamental modelocking are arguably limited. Microchip resonators reach extremely high repetition rates, but fundamentally, they are not lasers, and, practically, they offer no realistic paths to high powers [5, 6]. The alternative to shortening the cavities is harmonic modelocking, where the cavity simultaneously harbours multiple, ideally identical and equidistant, pulses [7]. In active harmonic modelocking, an externally driven modulator placed in the cavity localises the pulses equidistantly [7], but these lasers generate long pulses with low energies [8]. In passive harmonic modelocking [9], the pulses are

Mesut Laçin, Paul Repgen, Aladin Şura have contributed equally to this work.

✉ Fatih Ömer Ilday
ilday@bilkent.edu.tr

[1] Department of Physics, Bilkent University, 06800 Ankara, Turkey

[2] UNAM-National Nanotechnology Research Center and Institute of Materials Science and Nanotechnology, Bilkent University, 06800 Ankara, Turkey

[3] TÜBİTAK National Metrology Institute (UME), 41470 Kocaeli, Turkey

[4] Department of Electrical and Electronics Engineering, Bilkent University, 06800 Ankara, Turkey

self-organised through mutual nonlinear interactions that lead them to attract or repel each other, but the interaction mechanisms need to be better understood and are evidently only weakly binding [9–11]. Consequently, such lasers suffer from various instabilities. Even when the laser momentarily operates as intended, its harmonic state is easily disrupted by environmental perturbations. Harmonic modelocking has had a limited impact outside the laser research laboratory to date, but its utility can be improved significantly if its reliable, repeatable, and stable operation can be ensured.

We start by scrutinising how the different pulse fluctuations affect the purity of the harmonic operation. After finding out that deviations from equidistant temporal positions are more critical than variations in their energies, we relate the evolution of these deviations to the intrinsic laser noise by building an intuitive analogy to the motion of a Brownian particle trapped in a potential well. This model reveals how to suppress the deviations and improve the harmonic state, as quantified by the supermode suppression ratio, SSR, by implementing a band-pass filter (BPF) and increasing the intracavity pulse energy. Finally, we build a laser guided by these findings and experimentally attain record-high SSR. As we embark on a research programme to scale the repetition rates well into the high gigahertz levels with nanojoule-level pulse energies, the present contribution is a first step toward understanding the physics of the current paradigm. The achieved repetition rates are consequently modest, as no particular attempt was made to reach higher. Nevertheless, this may well be the first harmonically modelocked laser to perform comparably to a fundamentally modelocked fibre laser when judged by the purity of its repetition frequency, pulse energy, duration, noise characteristics, seemingly indefinite long-term stability of its harmonic state and excellent robustness against environmental perturbations.

2 Concept

2.1 Supermodes

We begin our exploration by analysing how imperfections in a harmonic state manifest. A pure harmonic state corresponds to perfectly equidistant and identical pulses. Let the number of such pulses be N. In such an ideal state, the harmonic operation is indistinguishable from fundamental modelocking. In the radio-frequency (RF) spectrum, the signals at the cavity's fundamental repetition rate, f_c, and its harmonics up to and excluding the Nth vanish. Only the operational repetition rate, $f_R = Nf_c$, and its harmonics remain. In practice, there are always deviations in the amplitude (pulse energy) or temporal positions of the pulses. These induce additional signals at f_c because the deviation is generally repetitive at each round-trip but also at the other harmonics, which appear in the form of supermode noise spurs [8]. As an example, the emergence of supermodes caused by a 0.1% deviation of only one pulse from the others in pulse energy and temporal position (in ratio to the ideal pulse-to-pulse distance) is illustrated in Fig. 1a. In general, all N pulses suffer different deviations. The supermode suppression ratio (SSR) is a convenient measure of the degree of deviation from the ideal harmonic state. Not all authors define it precisely or in the same way. We define it as the ratio of RF intensity at the harmonic repetition rate to that of the strongest supermode below the harmonic repetition rate, f_R. Reported SSR values in the literature are commonly in the range of 30–50 dB [10–15], although higher SSR values of 60 dB [16] and 70 dB [17] have been reported.

We first inquire about the respective contributions of temporal and amplitude deviations to the SSR. Their relative effects can be assessed perturbatively using the Fourier transform, which is given in Appendix 1, which shows that temporal deviations contribute significantly more for the same fractional amount. This is easy to appreciate: While a deviation of the pulse energy, δ_E, gives rise to supermodes with powers that depend on the ratio of the energy mismatch relative to the energy of all the pulses, the deviation in the pulse position, δ_τ, creates supermodes in the order of beating with an additional pulse in the pattern. This is easily verified by a numerical evaluation of the Fourier transform of the pulse pattern, as illustrated in Fig. 1a.

The temporal fluctuations not only contribute more to the SSR than amplitude variations, but also tend to be larger. Unlike pulse energy variations, which are controlled and suppressed effectively by self-amplitude modulation of the saturable absorber, deviations in the temporal positions can only be corrected by the pulse-to-pulse interactions, which are weak and act over nanoseconds-long delays. The weakness of these interactions is experimentally evidenced by the slow evolution of the pulse positions. The reorganisation of a perturbed pulse pattern can easily last many seconds [18] or even minutes [19]. This large timescale implies that the pulse-to-pulse interactions allow the pulse position displacements to accumulate from noise over typically millions or billions of roundtrips. In contrast, even a weak saturable absorber with a modulation depth of a few percent, suppresses the energy deviations within tens of roundtrips. Therefore, the main focus for improving the harmonic modelocking must lie on the damping of the fluctuations of the temporal positions of the pulses.

2.2 Analogy to a Brownian particle in an optical trap

One of the best-understood examples of a stochastic system at thermal equilibrium is a Brownian particle, i.e., a microscopic particle suspended in a fluid [20–22]. In recent

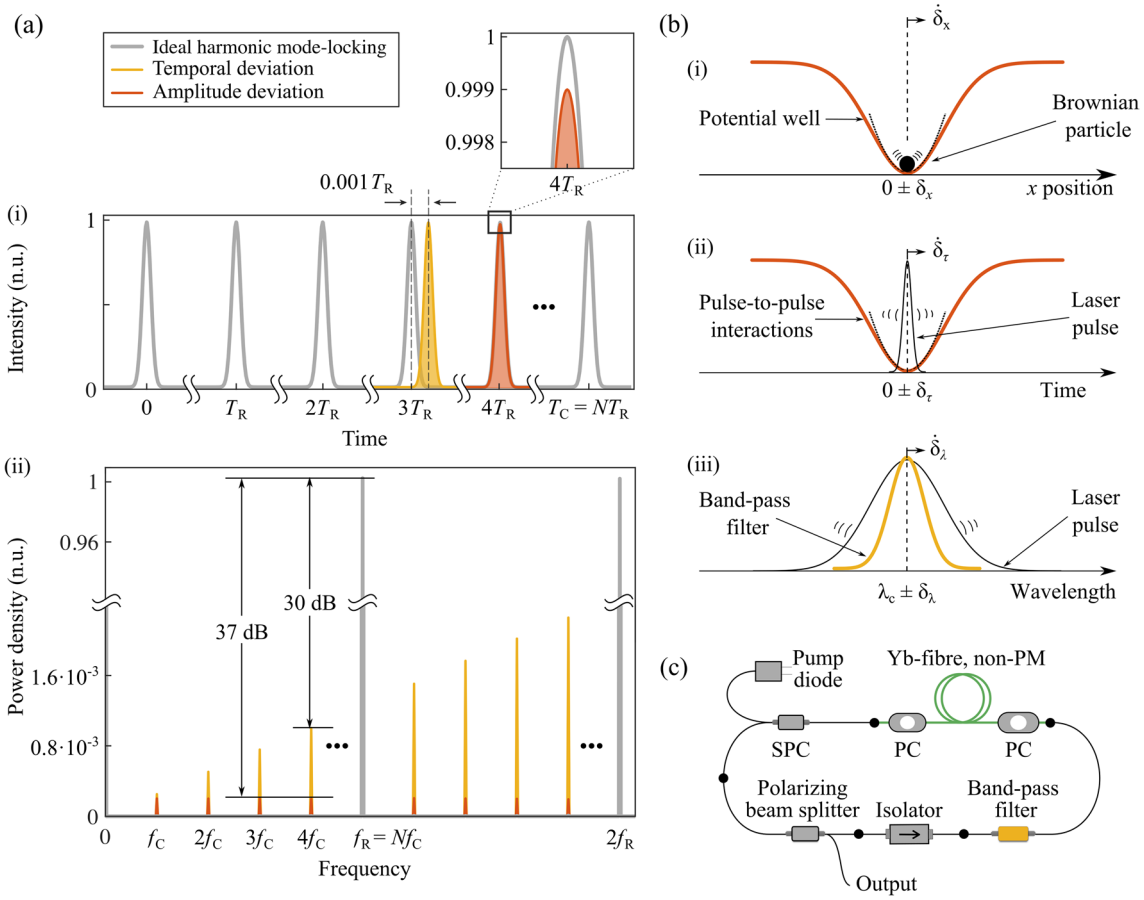

Fig. 1 **a** The supermodes are generated through the temporal displacement of one or more pulses in the harmonic pulse train (indicated red) or, less significantly, through an amplitude deviation (yellow). In the frequency domain, the supermodes show up at the fundamental repetition rate and its harmonics less than the *N*th. Shown is the numerical evaluation of 0.1% deviation in amplitude and temporal position for one pulse. **b** Similar to the damping of the motion of a Brownian particle in a potential well (orange), an optical pulse is kept in its temporal position through pulse-to-pulse interactions and the spectral filter, damping temporal deviations that could add up over multiple round trips due to dispersion. **c** The laser cavity is completely fibre-integrated and consists of polarisation-maintaining components except for the gain fibre for environmental robustness. *BPF* band-pass filter, *LD* pump laser diode, *PBS* fibre-integrated polarising beam splitter, *PC* polarisation controller, *SPC* signal-pump combiner

decades, the dynamics of optically trapped Brownian particles have been studied [23]. Their motion is described by a Langevin equation of the form,

$$m\ddot{x} = -\gamma\dot{x} + \kappa x + \sqrt{2k_B T\gamma}\xi(t), \tag{1}$$

where m is the mass, γ is damping due to fluid viscosity, κ is the stiffness of the restoring force due to the trap, simplified to be harmonic, k_B is the Boltzmann constant, T is the temperature, and $\xi(t)$ is a stochastic term describing white noise. The strength of the random collisions of the fluid molecules with the particle scales with T. A free Brownian particle undergoes a random walk, and as such, its mean square displacement, MSD, increases with time linearly, as opposed to quadratically for non-random motion, which is known as ballistic motion. A trapped particle explores a limited range around the centre of the trap. The MSD still increases linearly with time early on but plateaus at later times as higher displacement encounters a stronger restoring force. The MSD plateau is given by $k_B T/\kappa$, i.e. the stiffer the trap, the more subdued the particle's random motion is, as to be expected intuitively.

The analogy between the Brownian particle and the temporal fluctuations in a harmonically modelocked laser is presented in Fig. 1b. For simplicity, we focus on a single pulse out of the N pulses, but the same picture holds independently for any and every pulse. The deviations from the ideal harmonic state, especially the random temporal displacement from the pulses' positions of equal distance, are analogous to the Brownian motion of a trapped particle. Passive harmonic modelocking is onset by pulse-to-pulse interactions. Despite the decades-long interest, there is no consensus on their mechanisms. It is likely that multiple of the proposed ones are, respectively, valid for the laser cavities for which

they were proposed. For our purposes, the exact mechanism is not critical. The important point is that the interactions act like a trap, working to restore any deviating pulse towards its ideal temporal position, whereas laser noise continuously causes their positions to fluctuate. The result is a stochastic and dynamic steady state, where the average position of the pulse is the centre of the trap but the pulse undergoes random variations around it. The strength of the pulse-to-pulse interactions corresponds to the trap stiffness, κ. The laser noise causing the temporal fluctuations is analogous to the white noise of the Brownian motion and could be characterised by an effective temperature. There are multiple noise sources affecting the pulse position, including quantum fluctuations or amplified spontaneous emission (ASE), thermal noise, coupling of amplitude or shape fluctuations to temporal fluctuations through nonlinear pulse shaping, and possibly even environmental noise, although the latter is unlikely to affect pulses differently due to its slow time scale.

In Brownian motion, diffusivity characterises the strength of the random walk, and it is inversely proportional to the viscosity in the famous Einstein relationship, and for a trapped particle, increasing stiffness limits the range of walk-offs to smaller values. This analogy clarifies, in an intuitive manner, how to reduce the temporal walk-offs and increase the SSR in a laser: stronger pulse-to-pulse interactions and stronger filtering. The former would help the most directly, but in practice, we lack control over the interactions, which are not well understood at present. We would venture that synthetic pulse-to-pulse interactions based on well-known nonlinear optical processes could be conceived of in the future, and they could be highly effective, similar to how artificial saturable absorbers such as nonlinear polarisation evolution [24] or nonlinear optical loop mirrors [25] are more readily configurable and offer deeper modulation and faster recovery than saturable absorbers based on actual absorption in materials such as semiconductors. However, here, we focus on exploiting strong filtering as an effective path to higher SSR.

There is a long tradition of attributing particle-like properties to pulses, as portrayed by the suffixes of solitons and similaritons. Despite their certain particle-like characteristics, pulses are, of course, not particles and can undergo an evolution that has no counterpart in particles. The present analogy renders the fluctuations intuitive through the more familiar concepts of a Brownian particle, but the aspects through which the analogy deviates are also informative. One of them is that a pulse can be created and annihilated, unlike a Brownian particle. The former is the mechanism of the onset of harmonic modelocking, and together with the latter, it allows switching between harmonic states. It appears to be possible to precisely control the annihilation and creation of the pulses, but it requires a different laser cavity design and this is a direction that will be explored in a future article.

2.3 A Langevin equation for the pulse fluctuations

A major contribution to pulse position displacement is a fluctuation, δ_λ, of the central wavelength (in wavelength units) of the pulse induced by noise. A wavelength displacement of one pulse with respect to the others causes a relative temporal displacement, δ_τ (dimensionless), due to the total integrated dispersion of the cavity, D (in ps/nm), by an amount given by the dispersion equation [26]. A wavelength shift due to optical noise, mainly from ASE, is akin to velocity added to the Brownian particle by the collisions with the fluid molecules. Dissipative fluid viscosity reduces the velocity. For the optical pulse, spectral filtering is the viscous effect, reducing the wavelength shift. Stronger filtering dissipates the wavelength shift faster, just as a more viscous fluid dampens the Brownian particle's movement. A narrow spectral BPF in the cavity resets the spectral evolution each round-trip and, thus, minimises the spectral fluctuations, δ_λ. This minimisation is a dissipative damping of the temporal position deviations, δ_τ, each round-trip (see also Fig. 1b).

Next, we build up the qualitative analogies discussed above more formally. Although noise can cause temporal displacement directly by asymmetric reshaping of the pulse in the time domain, the dominant effect is due to deviations in their central wavelengths for a laser cavity with non-zero net dispersion, because the temporal displacement accumulates as long as the wavelength remains shifted with respect to the other pulses, even without further contributions from noise, just as a Brownian particle until an impulse into the opposite direction occurs. Ignoring the former, the speed of the temporal walkoff per roundtrip, $\dot{\delta}_\tau$, is given by

$$T_\mathrm{R}\dot{\delta}_\tau = \frac{D}{T_\mathrm{c}}\delta_\lambda, \tag{2}$$

where δ_τ is the deviation of the pulse position relative to T_R, which is the temporal distance between consecutive pulses in the ideal harmonic modelocking state, $T_\mathrm{c} = 1/f_\mathrm{c}$ is its roundtrip time, and f_c is the fundamental repetition rate. The central wavelength deviation, δ_λ, evolves under the effect of the noise, the spectral filtering, and the pulse-to-pulse interactions. We will discuss each of these.

We consider the principal noise source affecting the central wavelengths of the individual pulses differently to be ASE, which has a minimum value mandated by quantum fluctuations. There are numerous other noise sources, including environmental, but most of them simply affect all the pulses equally, as their amplitudes are weakened very strongly at the 100 MHz or even higher frequencies that are needed to cause differences between the individual

pulses. The interaction between ASE photons and the coherent pulses is analogical to the collisions of fluid molecules with a Brownian particle. Accordingly, we model the contribution of the noise to δ_λ as $\Delta\omega_\mathrm{p}\sqrt{h\nu/E_\mathrm{p}T_\mathrm{c}}\xi(t)$, where $\Delta\omega_\mathrm{p}$ is the spectral width of the pulse, h is Planck's constant, ν is the central frequency, E_p is the pulse energy at the entrance of the gain segment, and $\xi(t)$ is white noise with a variance of unity (with the unit $\mathrm{s}^{-1/2}$). The noise strength is inversely proportional to the number of photons contained within a pulse.

The filter reshapes the pulse spectrum of a wavelength-deviated pulse asymmetrically, pulling its centre toward that of the BPF. Even if there is no band-pass filter as an optical element, gain filtering fulfills this role, albeit weakly. For small deviations, the filter's effect is given by $-\alpha\delta_\lambda$, where α depends on the width of the filter and the spectrum. Assuming both to be Gaussians, $\alpha \approx \Delta\omega_\mathrm{p}^2/(\Delta\omega_\mathrm{f}^2+\Delta\omega_\mathrm{p}^2)T_\mathrm{c}^{-1}$ with $\Delta\omega_\mathrm{f}$ being the filter width.

We incorporate the effect of the pulse-to-pulse interactions phenomenologically with the term $-\kappa\delta_\tau T_\mathrm{R}$, because their exact nature is not known; for the cases of chirped pulses, any position adjustment by temporally asymmetric modulation (as would be by an amplitude modulator) necessarily creates a position-dependent wavelength shift for chirped pulses. Additionally, most pulse-to-pulse interaction mechanisms proposed in the literature involve direct position-dependent wavelength shifts. Here, κ is a proportionality constant that determines the strength of the interactions as the rate of shift of the central wavelength per unit of temporal displacement (with the unit nm/(ps s)).

Considering all of the three contributions, we arrive at a Langevin equation for the position of the central wavelength,

$$\dot{\delta}_\lambda = -\alpha\delta_\lambda - \kappa\delta_\tau T_\mathrm{R} + \Delta\omega_\mathrm{p}\sqrt{\frac{h\nu}{T_\mathrm{c}E_\mathrm{p}}}\xi(t). \tag{3}$$

Recasting this equation in terms of the temporal shift,

$$\frac{T_\mathrm{c}}{D}\ddot{\delta}_\tau = -\gamma\dot{\delta}_\tau - \kappa\delta_\tau + \frac{\Delta\omega_\mathrm{p}}{T_\mathrm{R}}\sqrt{\frac{h\nu}{T_\mathrm{c}E_\mathrm{p}}}\xi(t). \tag{4}$$

Here, we note that κ corresponds to the trap stiffness, $\gamma = \alpha T_\mathrm{c}/D$, which sets the filter strength, is the equivalent of fluid viscosity in Brownian motion. One difference from the Brownian case is that the strength of the noise is independent of the filtering for the pulses, whereas both the viscosity and the noise source are due to collisions with the fluid molecules for a Brownian particle. The factor T_c/D is equivalent to the effective mass. The smaller the mass, i.e. the larger the cavity dispersion, the less time is needed for the wavelength-shifting forces on the right-hand side to change the speed. This inertial term is commonly assumed to be negligibly small for Brownian particles. We will assess the validity of this assumption for pulses by comparing the coefficients of the inertial and viscous terms in adimensional forms, which we obtain by dividing by κ and expressing the time-derivatives in terms of the characteristic time $t_0 \equiv \gamma/\kappa$, which is the timescale of the evolution of the pulse positions. Then, the coefficient of the viscous term becomes one, while the coefficient of the inertial term becomes $T_\mathrm{c}/(D\kappa t_0^2) = 1/(\alpha t_0)$. Usually, the evolution of the pulse positions is slow enough that it can be observed on the oscilloscope or the RF spectrometer in real time. This means that the timescale of this evolution, t_0, is on the order of a second, which is typically on the order of 10^7 T_c. The parameter α varies with the spectral and filter widths, but even if the gain is the only filter and the pulse spectrum is as narrow as 10% of the gain bandwidth, α remains on the order of $0.01\ T_\mathrm{c}^{-1}$ or larger. Then, the (adimensionalised) coefficient of the inertial term is on the order of 10^{-5}; the inertial term is negligibly small. Physically, because the relative speeds of the pulses are typically very low, the positions of the pulses change only negligibly within the time it takes for a pulse to accelerate through the evolution of its wavelength. Consequently, the speed is determined by the pulse position and the noise at all times, except for negligibly brief transient acceleration.

After neglecting the inertial term, we arrive at our Langevin equation for the temporal fluctuations of a pulse in a harmonic modelocked laser,

$$\gamma\dot{\delta}_\tau = -\kappa\delta_\tau + \frac{\Delta\omega_\mathrm{p}}{T_\mathrm{R}}\sqrt{\frac{h\nu}{T_\mathrm{c}E_\mathrm{p}}}\xi(t). \tag{5}$$

This equation establishes our analogy formally. It is easy to see that in the absence of the noise term (valid for large deviations), the deviation experiences exponential decay with the time constant, $t_0 = \gamma/\kappa$.

2.4 Temporal fluctuations of a harmonic pulse and laser design considerations for their suppression

The temporal position fluctuations of a single pulse turn out to be formally like that of a trapped Brownian particle within our simple model (Eq. 5). The mean square displacement is,

$$\left\langle \left(\delta_\tau(t) - \delta_\tau(0)\right)^2 \right\rangle = \frac{\Delta\omega_\mathrm{p}^2}{2T_\mathrm{R}^2\gamma\kappa T_\mathrm{c}}\frac{h\nu}{E_\mathrm{p}}\left(1 - e^{-t/t_0}\right). \tag{6}$$

Here, t is the measurement time, and $t = 0$ corresponds to an instantaneous measurement, for which the MSD vanishes because the particle has not yet deviated from its position, which does not necessarily correspond to $\delta_\tau = 0$. Over longer times, the pulse position deviation increases, on

average with the square root of the elapsed time (measurement duration), but the deviation plateaus at a finite value given by,

$$\left\langle \delta_\tau^2 \right\rangle = \frac{\Delta\omega_\mathrm{p}^2}{2T_\mathrm{R}^2\gamma\kappa T_\mathrm{c}}\frac{h\nu}{E_\mathrm{p}}. \tag{7}$$

As expected from the trapped Brownian particle analogy, temporal fluctuations will be subdued if the trap created by the particle-to-particle interactions is stronger (large κ). However, this is difficult to manipulate experimentally, partly because the mechanism is not well known and further, assuming that the most likely candidate, namely acoustic interactions, is the mechanism responsible, material properties severely limit the possibilities. Nevertheless, we identify two other practical means of suppressing the fluctuations, both of which we will exploit experimentally. The first is that stronger filtering (large γ) dampens the fluctuations. The physical reason is straightforward; filtering reduces the rate of deviations. The second is that the intrinsic noise causing the central wavelength fluctuations scales inversely with the number of photons in a pulse. Thus, the higher the *intracavity* pulse energy, the smaller the fluctuations in the first place. Decreasing the cavity loss increases the pulse energy at the entrance of the gain, thus decreasing the sensitivity of the pulses to ASE. Once again, the physical reason is quite clear. Each random ASE photon perturbs the pulse, like fluid molecules hitting the Brownian particle. The larger the number of photons per pulse, the less is the impact on the pulse characteristics, including its central wavelength. Increasing the pulse energy might also indirectly help by increased nonlinear spectral broadening, which, in turn, is equivalent to stronger filtering, since $\gamma \propto \Delta\omega_\mathrm{p}^2/(\Delta\omega_\mathrm{f}^2 + \Delta\omega_\mathrm{p}^2)$, but a broader spectrum also strengthens the noise term, and its benefits are not clear. However, increasing the intracavity pulse energy may further help by strengthening the pulse-to-pulse interactions (increasing κ). This is to be expected even though we do not know the pulse-to-pulse interaction mechanisms precisely, because any pulse-to-pulse interaction must necessarily be nonlinear in origin.

Guided by the trapped Brownian particle analogy, we now discuss design considerations for and their practical implementation in a fibre laser cavity. The modelocking regimes that allow high pulse energies are similariton [27–30] and all-normal-dispersion (dissipative soliton) [31] regimes. However, the pulse energy can be limited also by overdriving the saturable absorber. In fact, a harmonic state is achieved precisely by pulse breakup that occurs by overdriving, so the laser's operation must necessarily be near such a point. But also, the pulses must experience strong nonlinearity to achieve broader pulse spectra for stronger filtering, without excessive overdriving of the saturable absorber. We have chosen nonlinear polarisation evolution (NPE) as the artificial saturable absorber due to its ease of implementation, nearly instantaneous response, strong modulation depth, and high peak transmission. NPE occurs only in non-polarisation-maintaining (non-PM) fibres, which we exploited to partially decouple NPE from the nonlinear evolution of the pulse by limiting the non-PM fibre to be short and building the rest of the cavity from PM fibres. The shorter the non-PM fibre, the higher the pulse energy must be to accumulate sufficient polarisation rotation for maximum transmission. This way, the pulse energy that overdrives NPE is set to considerably higher values. The polarising beam splitter in the NPE scheme functions both as a saturable absorber and as an output coupler, thus limiting the linear losses of the cavity.

There is a further practical benefit of this design. Much of the cavity comprises PM fibre, which is insensitive to thermal or vibrational environmental effects [32, 33]. These only affect the non-PM fibre by randomly inducing birefringence through mechanical stress. We chose the only non-PM fibre, where NPE occurs, to be the gain fibre, which was coiled to occupy a smaller area. The cavity is also entirely fibre-integrated to improve long-term stability by avoiding the possibility of mechanical misalignment. As will be discussed in the next section, this design results in self-starting operation with excellent long-term and environmental stability during harmonic modelocking.

Before discussing our experimental implementation, we finally remark on the alternative or complementary approach of setting the net cavity dispersion to zero, in which case the central wavelength fluctuations would not translate to temporal fluctuations. Apart from the practical difficulty that this can be accomplished only at a single wavelength due to the presence of large third-order dispersion in any fibre cavity, most cavities to date that achieved strong filtering and high pulse energies also had a high amount of net dispersion. There have been exceptions, including a laser design we have developed previously [34]. However, none were all-fibre-integrated nor particularly practical. We have decided to focus on a simple, compact, all-fibre implementation, but we remark that reducing the net dispersion is another likely improvement that could be explored in the future.

3 Experimental results

The setup is shown in Fig. 1c. As mentioned above, the Yb-doped double-clad gain fibre (nLight, Yb1200-6/125DC) is the only non-PM component in the oscillator cavity, has a length of 1.6m and is coiled and isolated by immersion in a soft polymer (Momentive, RTV6136-D1). The polarisation state is manipulated through two fibre-based polarisation controllers (PC) at the two ends of the gain fibre. The Yb-doped fibre is cladding-pumped through a signal-pump

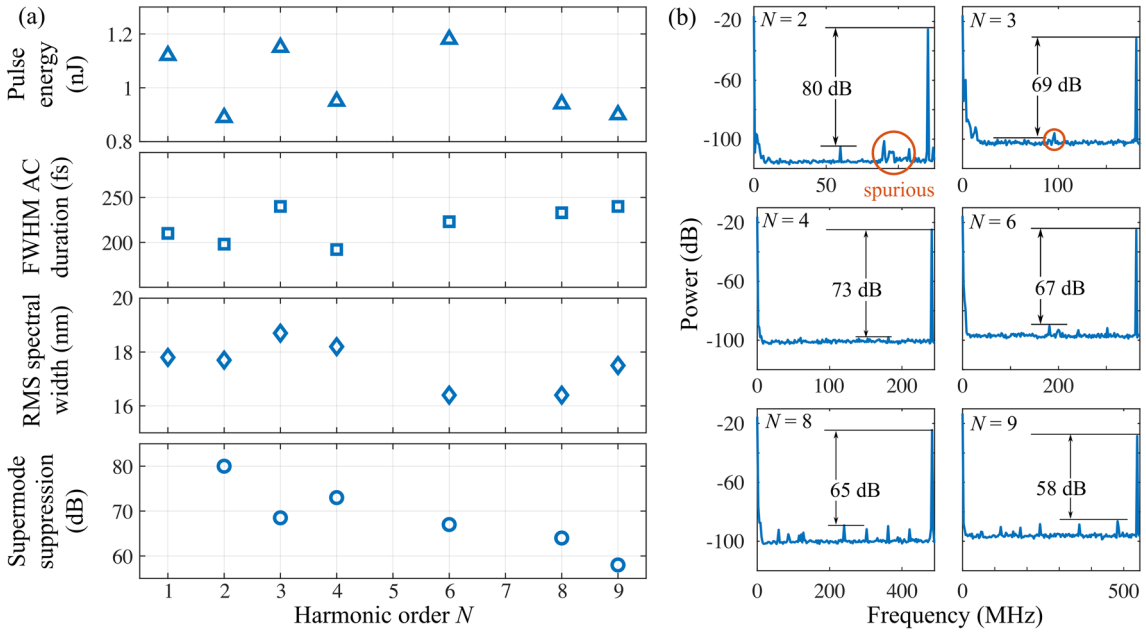

Fig. 2 Comparison of the operation parameters of different harmonic modelocked states (**a**). The supermode suppression values are taken from individual measurements at the different harmonic states. The respective RF traces are plotted in (**b**), spurious noise marked in orange for easier distinction

combiner by a wavelength-stabilised multimode pump diode operating at 976 nm wavelength. A fibre-integrated polarising beam splitter acts as a polarisation discriminator and the only output coupler. A fibre-based isolator sets the direction of signal propagation. A fibre-based Gaussian-shaped BPF with full-width at half-maximum (FWHM) width of 10 nm, centred at 1030 nm, provides the spectral filtering required for the dissipative soliton modelocking regime and dampens the Brownian-like temporal fluctuations of the pulses, as discussed above. The total fibre length of the cavity accumulates to 3.4 m with a corresponding fundamental repetition rate of 60.4 MHz.

We readily obtain self-starting modelocking, and can subsequently reach as high as the ninth harmonic repetition rate by an appropriate setting of the pump power and the PCs. The fact that the adjustment of the PCs lacks a clear algorithm is the most important shortcoming of this implementation, but it is common to all NPE-based lasers. All harmonic states are achieved at nearly the same pulse energy of 0.9 nJ, and higher harmonics are accessed by progressively increasing the pump power and overdriving the pulse energy to create one new pulse, accompanied by tiny corrections on the PCs. Once these settings are correctly adjusted, the pulse pattern approaches the new harmonic state, and the supermodes decay in the timescale of about a second. In one case, we recorded the settling of the pulse pattern in video and measured the rate of decay of the supermodes to be around 60 dB/s. Given the dependence of the supermode power on the temporal deviation (see Appendix 1), this decay rate implies the time constant for the attenuation of the deviation, t_0, to be around 0.14 s^{-1}.

The immediate limitation to the maximum harmonic number is due to the average power, which corresponds to an intracavity value of about 1 W for the ninth harmonic. This is already substantially higher than the power rating (300 mW) of the fibre-integrated components, which we did not want to strain any further and made no attempts to reach higher harmonics. For prolonged operation in our laboratory over the course of several months, we have settled at the sixth harmonic. An updated design using high-power components should readily reach higher harmonics.

The performances of the harmonic states of different orders are summarised in Fig. 2a. We adjusted the pump power for each harmonic state, such that the pulse energies are around 0.9 nJ for each harmonic state. The SSR roughly follows the measured spectral width of the respective harmonic state, as well as the FWHM of the AC duration. While the latter is apparently due to uncompressible nonlinear phase accumulated in the output fibres [35], the correlation of spectral width and the SSR implies the correlation of intracavity pulse energy with SSR since the larger spectral width requires higher pulse energies. This correlation is theoretically expected. The measured SSR values differ among the harmonic modelocking orders. In the harmonic order $N = 2$, we obtained a record value for the SSR of 80 dB (Fig. 2b).

The optical characteristics are broadly similar for all harmonic states. For the sake of brevity, we discuss the

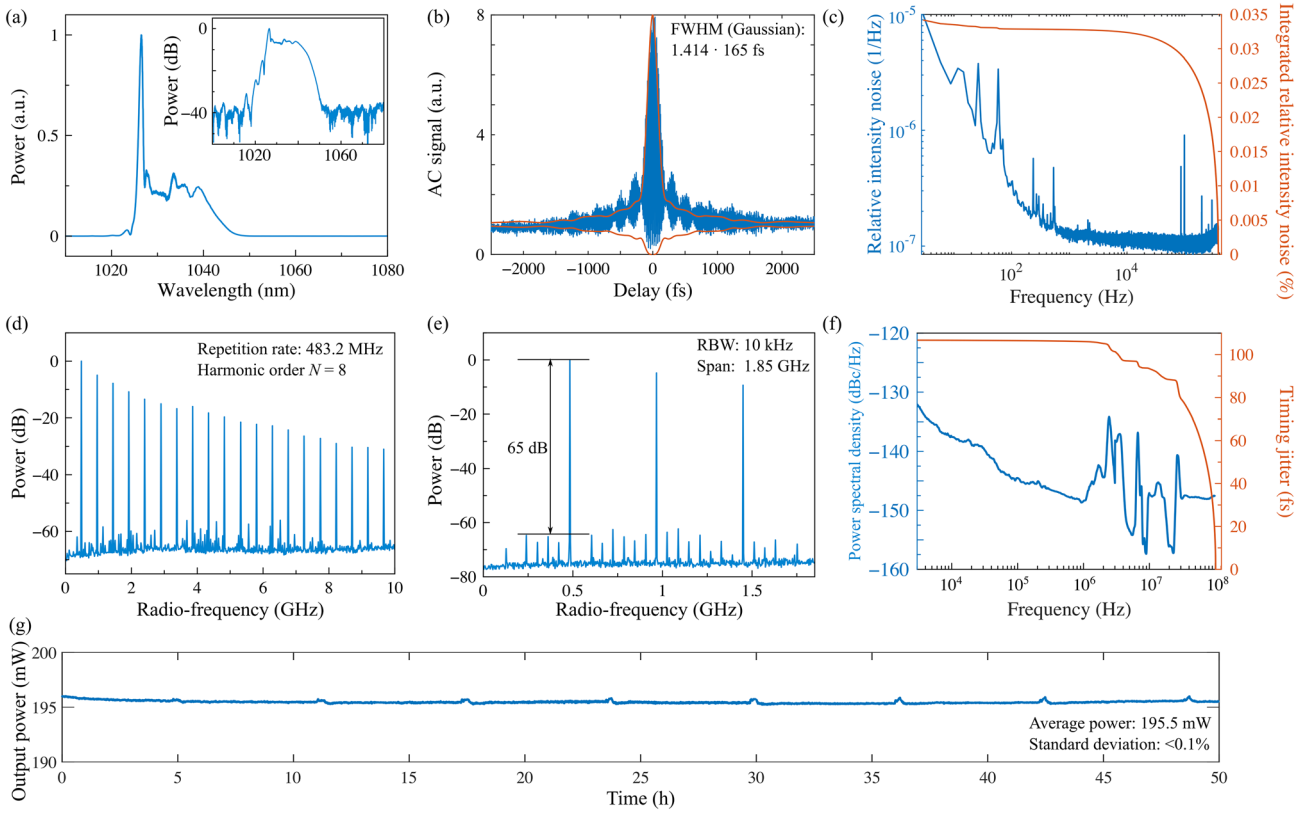

Fig. 3 Operation parameters at the eighth harmonic repetition rate, at 483 MHz: **a** spectral width, ranging over 16 nm in linear scale, with semi-logarithmic scale in the inset, **b** the autocorrelation trace of the compressed pulse (blue), with the calculated trace of the Fourier-transformed pulse in orange, **c** the relative intensity noise (blue) and the integrated relative intensity noise (orange), **d** the long-range radiofrequency trace, **e** a shorter radiofrequency trace to evaluate the suppression of supermodes, and **f** the phase noise measurement (blue) and the integrated timing jitter between 1 kHz and 100 MHz. The laser has a stable output power **g** over the course of more than 50 h. We confirmed independently that the spikes in the signal result from a systematic error in the pump diode that causes spikes in its output power

eighth harmonic, at 484 MHz, in detail (Fig. 3). The root-mean-square (RMS) spectral bandwidth is 16.4 nm (Fig. 3a). Using a pair of 900 lines/mm-gratings, the output pulses can be compressed from 7.7 ps to 233 fs of autocorrelation (AC) duration (Fig. 3b), corresponding to a FWHM of 165 fs, assuming a Gaussian pulse shape, which is 31% longer than the transform-limited duration (126 fs). We also characterized the short-term stability by relative intensity noise (RIN) and phase noise measurements. For the former, we used a photodiode with 150 MHz bandwidth and additionally filtered the electrical signal with a low-pass filter with 1.9 MHz cut-off, which was analysed with a baseband spectrum analyser (Rohde & Schwartz UPV). The integrated noise is obtained by integrating the measured noise spectrum over the desired bandwidth, multiplying by 2 (to account for the double sidebands), and taking the square root. The double-sided RIN integrated from between 3 HZ to 250 kHz amounts to 0.034% (Fig. 3c). This value is comparable to fundamentally modelocked fibre oscillators pumped in core by singlemode diodes [36] and remarkably low considering the higher noise of multimode pump laser diodes [37]. The wider-range RF spectrum (Fig. 3d) shows smoothly decaying maxima, indicating the absence of bound pulses, which were also ruled out by long-range AC measurements. When the laser operates in the eighth harmonic state, the intensity of the supermodes is suppressed by at least 65 dB compared to the first beat node (Fig. 3e). Phase noise was measured at the second harmonic of the free-running (harmonic) repetition frequency (968 MHz) in the RF spectrum using a signal source analyser (Rohde & Schwartz FSUP26). The timing jitter in the eighth harmonic is calculated to be 106 fs (Fig. 3f) by integrating the phase noise from 100 MHz down to 1 kHz. In this state, the average output power of the laser was 450 mW, corresponding to 0.9 nJ pulse energy. The output was stable, seemingly indefinitely; a continuous measurement over the course of two days is provided in Fig. 3g.

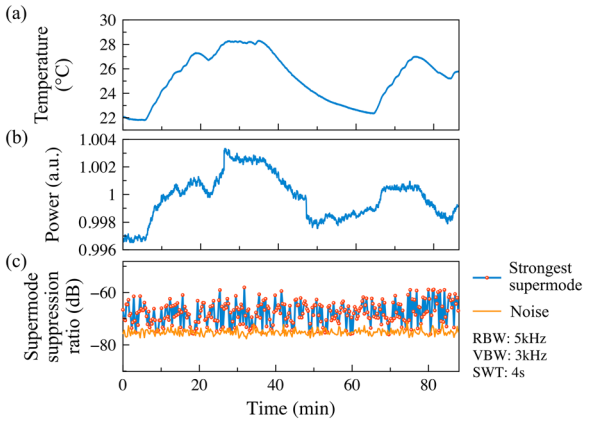

Fig. 4 Long-term environmental test of the laser oscillator, operating in the 6th harmonic state, at 362 MHz. The temperature is cycled for around 6°C over 90 min (**a**). Despite the deliberately applied strong environmental temperature change, the output power (**b**), normalised around the mean value, fluctuates with a standard deviation of 0.17%. The ratio from the first beat node in the RF spectrum to the strongest supermode maximum (**c**) has an average of 67.9 dB and shows no dependency on the temperature. *RBW* resolution bandwidth, *SWT* sweep time, *VBW* video bandwidth

Benefiting from the all-fibre design, the isolation of the gain fibre and the dominance of PM fibres, the oscillator also shows excellent long-term stability and environmental robustness. The output power varied less than 0.07% over a duration of 50 h in the eighth harmonic state (Fig. 3g). We also deliberately induced large changes in the temperature of the laser to verify its environmental stability. While the laser was operating in the sixth harmonic state, the temperature was varied by 6 °C over the course of 90 min by applying a heat source externally. Such a temperature variation is much more than expected in a laser laboratory. Despite that, the harmonic state was never interrupted. The results are depicted in Fig. 4. While the output power (Fig. 4b) shows a slight dependence on the temperature (Fig. 4a), there is no measurable effect on the laser performance. The AC and optical spectrum measurements did not indicate any changes. Despite the large temperature change, the pulse energy remained constant at 0.9 nJ with a standard deviation of less than 0.2%. Even these small changes in power appear to be originating entirely from the pump laser's output wavelength varying with temperature despite being nominally wavelength stabilised. Over time, the relative strength of the supermodes changes randomly between the noise floor of our measurement and the SSR 60 dB, but always remaining high, with a mean value of 67.9 dB (Fig. 4c). These fluctuations in the supermodes' powers largely reflect the stochastic nature of the pulse position deviations but also, to a lesser extent, the measurement capability of our equipment. Overall, the purity of the harmonic state, as quantified by the supermode suppression, shows no discernable dependence on environmental disturbances.

4 Conclusion

In summary, we present a theoretical analysis of the origins of fluctuations in harmonic modelocking, which reveals a formal and intuitive analogy to a trapped Brownian particle. Guided by the insights provided by the analogy, we built a passively harmonic modelocked fibre laser that achieved excellent operational characteristics. It is an entirely fibre-integrated laser, employing mostly polarisation-maintaining fibres everywhere except the gain fibre, where the nonlinear polarisation evolution is confined to a non-polarisation-maintaining short section. This way, higher intracavity pulse energies are tolerated by increasing the energy that overdrives the saturable absorber. The laser achieves record-high supermode suppression ratio values up to 80 dB, but even more importantly, its harmonic state is completely robust over prolonged operation measured over more than 50 h. Even in the presence of unusually large changes in the environmental temperature of 6 °C, the harmonic state remains unperturbed. The measured timing jitter is 106 fs, based on integrating the phase noise between 100 MHz and 1 kHz. This level of timing jitter is also an order of magnitude below that of other passively harmonic modelocked lasers. The present laser's optical power was limited by the power handling in the fiberised components, specifically the polarisation beam splitter and the band-pass filter. With superior components, higher repetition rates should be reachable.

Overall, we present what we believe to be the first harmonically modelocked laser to operate similarly to a typical fundamentally modelocked fibre laser without notable trade-offs in any important aspect, namely, short-term stability, quantified by phase and relative intensity noise, long-term stability, including being subjected to temperature variations, pulse energy, pulse duration, and average power (up to 1 W). The design does not rely on special components, making it easy to duplicate. We expect it to find use in applications requiring high repetition rates, including as a stable seed source for ablation-cooled material processing in the GHz regime [2, 38].

Contributions of energy and position deviations to the supermode suppression ratio

The radio-frequency (RF) signal is the Fourier transform of the time signal. The RF trace, at frequency f in logarithmic scale, is

$$\mathrm{RF}(f) = 10\log_{10}\left(C \times |\tilde{P}(f)|^2\right)$$

$$|\tilde{P}(f)|^2 = \left|\frac{1}{T_\mathrm{c}}\int_0^{T_\mathrm{c}} \exp\left(-2\pi \mathrm{i}\frac{n}{T_\mathrm{c}}\tau\right)\sum_{j=1}^{N} E_j u(\tau-\tau_j)\mathrm{d}\tau\right|^2. \tag{A1}$$

Here, $\tilde{P}(f)$ is the Fourier transform of the photocurrent from the photodiode, C is a proportionality constant adding a vertical shift to the RF trace, T_c is the cavity round-trip time, n is a positive integer enumerating the maxima in the RF trace such that $f_n = n/T_\mathrm{c}$ represents all frequencies allowed by the periodicity of the cavity. Furthermore, τ is the delay coordinate, N is the number of pulses in the cavity, E_j and τ_j are the energy and temporal position of the jth pulse, respectively, and u describes the temporal profile of the electrical current pulse generated by the photodetector in response to an optical pulse as measured by the RF spectrum analyser. Approximating the electrical pulse shape u as a delta function leads to

$$|\tilde{P}(f)|^2 = \left|\frac{1}{T_\mathrm{c}}\sum_{j=1}^{N} E_j \exp\left(-2\pi \mathrm{i}\frac{n}{T_\mathrm{c}}\tau_j\right)\right|^2. \tag{A2}$$

With N identical pulses in the cavity (Nth harmonic state), each with an energy E, and positioned equidistantly ($\tau_j = jT_\mathrm{c}/N$), the Fourier transform becomes

$$|\tilde{P}(f)|^2 = \left(\frac{NE}{T_\mathrm{c}}\right)^2, \tag{A3}$$

if n/N is an integer, otherwise zero. The maxima in the RF trace at frequencies n/T_c other than integer multiples of N/T_c result from supermodes. The supermode-maxima only appear in case of deviations from the ideal pulse train. A relative (fractional) energy deviation of δ_E in one pulse (e.g., the first pulse, $j = 1$) leads to

$$|\tilde{P}(f)|^2 = \left(\frac{E}{T_\mathrm{c}}\delta_\mathrm{E}\right)^2, \tag{A4}$$

if n/N is not an integer (at supermodes),

$$|\tilde{P}(f)|^2 = \left(\frac{E}{T_\mathrm{c}}(N+\delta_E)\right)^2,$$

if n/N is an integer (at the harmonic repetition rate). (A5)

The supermode suppression ratio (SSR) (in logarithmic scale) due to the energy deviation is the ratio between Eqs. A4 and A5:

$$\mathrm{SSR} = 10\log_{10}\left(\frac{|\tilde{P}(N/T_\mathrm{c})|^2}{|\tilde{P}(n/T_\mathrm{c})|^2}\right) = 10\log_{10}\left(\left(\frac{N}{\delta_E}+1\right)^2\right) \approx 20\log_{10}\left(\left|\frac{N}{\delta_E}\right|\right), \tag{A6}$$

$$\delta_E = \frac{1}{N}\times 10^{-\frac{\mathrm{SSR}}{20}}, \tag{A7}$$

where n corresponds to the supermode for which the SSR is to be measured. In the case of a position deviation δ_τ in the first pulse, by linearizing with respect to δ_τ, $|\tilde{P}(f)|^2$ becomes

$$|\tilde{P}(f)|^2 \approx \left(2\pi\frac{n}{T_\mathrm{c}^2}\delta_\tau T_\mathrm{R} E\right)^2 = \left(\frac{E}{T_\mathrm{c}}\right)^2\left(2\pi\frac{n}{N}\delta_\tau\right)^2, \tag{A8}$$

if n/N is not an integer (at supermodes)

$$|\tilde{P}(f)|^2 \approx \left(\frac{E}{T_\mathrm{c}}\right)^2\left(\left(2\pi\frac{n}{N}\delta_\tau\right)^2 + N^2\right), \tag{A9}$$

if n/N is an integer.

The resulting SSR then is again the ratio of Eqs. A8 and A9:

$$\begin{aligned}\mathrm{SSR} &= 10\log_{10}\left(\frac{|\tilde{P}(N/T_\mathrm{c})|^2}{|\tilde{P}(n/T_\mathrm{c})|^2}\right)\\ &= 10\log_{10}\left(\frac{\left(\frac{E}{T_\mathrm{c}}\right)^2\left(\left(2\pi\frac{n}{N}\delta_\tau\right)^2+N^2\right)}{\left(\frac{E}{T_\mathrm{c}}\right)^2\left(2\pi\frac{n}{N}\delta_\tau\right)^2}\right)\\ &\approx 20\log_{10}\left(\left|\frac{N^2}{2\pi n}\frac{1}{\delta_\tau}\right|\right),\end{aligned} \tag{A10}$$

$$\delta_\tau = \frac{2\pi n}{N^2}\times 10^{-\frac{\mathrm{SSR}}{20}}. \tag{A11}$$

Acknowledgements The authors acknowledge Ghaith Makey for support in the automatisation of the data acquisition. This work received funding from the European Research Council (ERC) under the European Union's Horizon 2020 research and innovation programme (SUPERSONIC and UniLase with grant agreements No. 966846 and No. 101055055, respectively) and TÜBİTAK (Grant agreement No. 20AG024).

Declarations

Conflict of interest The authors declare no competing interests.

References

1. L.E. Hargrove, R.L. Fork, M.A. Pollack, Appl. Phys. Lett. **5**, 4 (1964)
2. C. Kerse, H. Kalaycıoğlu, P. Elahi, B. Çetin, D.K. Kesim, Ö. Akçaalan, S. Yavaş, M.D. Aşık, B. Öktem, H. Hoogland, R. Holzwarth, F.Ö. Ilday, Nature **537**, 84 (2016)
3. N. Ji, J.C. Magee, E. Betzig, Nat. Methods **5**(2), 197–202 (2008). https://doi.org/10.1038/nmeth.1175
4. B.W. Tilma, M. Mangold, C.A. Zaugg, S.M. Link, D. Waldburger, A. Klenner, A.S. Mayer, E. Gini, M. Golling, U. Keller, Light Sci. Appl. **4**, e310 (2015)

5. T.J. Kippenberg, A.L. Gaeta, M. Lipson, M.L. Gorodetsky, Science **361**, 8083 (2018)
6. B. Stern, X. Ji, Y. Okawachi, A.L. Gaeta, M. Lipson, Nature **562**, 401 (2018)
7. H.A. Haus, IEEE J. Quantum Electron. **11**, 323 (1975)
8. F. Quinlan, S. Gee, S. Ozhara, P.J. Delfyett, IEEE Photon. Technol. Lett. **19**, 1221 (2007)
9. F. Amrani, A. Niang, M. Salhi, A. Komarov, H. Leblond, F. Sanchez, Opt. Lett. **36**, 4239 (2011)
10. A. Hause, H. Hartwig, M. Böhm, F. Mitschke, Phys. Rev. A **78**, 063817 (2008)
11. R. Weill, A. Bekker, V. Smulakovsky, B. Fischer, O. Gat, Optica **3**, 189 (2016)
12. V.A. Ribenek, D.A. Korobko, A.A. Fotiadi, J.R. Taylor, Opt. Lett. **47**, 5236 (2022)
13. S. Zhou, D.G. Ouzounov, F.W. Wise, Opt. Lett. **31**, 1041 (2006)
14. B. Ortaç, A. Hideur, G. Martel, M. Brunel, Appl. Phys. B **81**, 507 (2005)
15. C. Lecaplain, P. Grelu, Opt. Express **21**, 10897 (2013)
16. J. Wang, X. Bu, R. Wang, L. Zhang, J. Zhu, H. Teng, H. Han, Z. Wei, Appl. Opt. **53**, 5088 (2014)
17. B. Piechal, T.M. Kardas, M. Pielach, Y. Stepanenko, Stable harmonic mode locking in all PM-Fiber Mamyshev oscillator. Conference on Lasers and Electro-optics, SW3R.4. https://doi.org/10.1364/CLEO_SI.2020.SW3R.4
18. A.B. Grudinin, S. Gray, J. Opt. Soc. Am. B **14**, 144 (1997)
19. B. Ortaç, A. Hideur, M. Brunel, Opt. Lett. **29**, 1995 (2004)
20. R. Brown, Philos. Mag. **4**, 161 (1827)
21. A. Einstein, Ann. Phys. **322**, 549 (1905)
22. H. Haken, H. Sauermann, C. Schmid, H.D. Vollmer, Z. Phys. **206**, 369 (1967)
23. G. Volpe, D. Petrov, Phys. Rev. Lett **97**, 210603 (2006)
24. V.J. Matsas, T.P. Newson, M.N. Zervas, Opt. Commun. **92**, 61 (1992)
25. N.J. Doran, D. Wood, Opt. Lett. **13**, 56 (1988)
26. G.P. Agrawal, *Nonlinear Fiber Optics*, 4th edn. (Elsevier Inc., 2004)
27. F.Ö. Ilday, J.R. Buckley, W.G. Clark, F.W. Wise, Phys. Rev. Lett. **92**, 213902 (2004)
28. W.H. Renninger, A. Chong, F.W. Wise, Phys. Rev. A **82**, 021805 (2010)
29. W.H. Renninger, A. Chong, F.W. Wise, Opt. Express **19**, 22496 (2011)
30. B. Oktem, C. Ülgüdür, F.Ö. Ilday, Nat. Photon **4**, 307 (2010)
31. A. Chong, J. Buckley, W. Renninger, F. Wise, Opt. Express **14**, 10095 (2006)
32. M. Erkintalo, C. Aguergaray, A. Runge, N.G.R. Broderick, Opt. Express **20**, 22669 (2012)
33. M. Pielach, B. Piechal, J. Szczepanek, P. Kabacinski, Y. Stepanenko, IEEE Access **8**, 145087 (2020)
34. Ç. Şenel, R. Hamid, C. Erdoğan, M. Çelik, F.Ö. Ilday, Phys. Rev. Appl. **10**, 1 (2018)
35. D. Mortag, D. Wandt, U. Morgner, D. Kracht, J. Neumann, Opt. Express **19**, 546 (2011)
36. I.L. Budunoğlu, C. Ülgüdür, B. Oktem, F.Ö. Ilday, Opt. Lett. **34**, 42916 (2009)
37. K. Gürel, P. Elahi, L. Budunoğlu, Ç. Şenel, P. Paltani, F.Ö. Ilday, Appl. Phys. Lett. **105**, 011111 (2014)
38. P. Elahi, H. Kalaycıoğlu, Ö. Akçaalan, C. Ertek, K. Eken, F.Ö. Ilday, Opt. Lett. **43**, 535 (2018)